Progress In Electromagnetics Research B, Vol. 55, 401–419, 2013

EFFECTS OF MICROELECTRODE ARRAY CONFIGURATION AND POSITION ON THE THRESHOLD IN ELECTRICAL EXTRACELLULAR STIMULATION OF SINGLE NERVE FIBER: A MODELING STUDY

Xin-Tai Zhao[1], Zhi-Gong Wang[1, *], and Xiao-Ying Lü[2]

[1]Institute of RF- & OE-ICs, Southeast University, Nanjing 210096, China

[2]State Key Laboratory of Bioelectronic, Southeast University, Nanjing 210096, China

Abstract—A transient finite-element model has been presented to simulate extracellular potential stimulating in a neural tissue by a nonplanar microelectrode array (MEA). This model allows simulating the extracellular potential and transmembrane voltage by means of a single transient computation performed within single finite element (FE) software. The differential effects of the configuration and position of MEA in electrical extracellular stimulation are analyzed theoretically. 3-D models of single nerve fiber and different MEA are used for the computation of the stimulation induced field potential, whereas a cable model of a nerve fibre is used for the calculation of the transmembrane voltage of the nerve fiber. The position of MEA and the spacing of the microelectrodes are varied while mono-, bi-, tri-, and penta-polar MEAs are applied. The model predicts that the lowest stimulation voltage threshold is obtained in the stimulation with penta-polar MEA. Moreover, the relationships, which exist between the thresholds of the electrical extracellular stimulation and the parameters including position of the electrode array and the spacing of the microelectrodes in array, are studied and obtained.

1. INTRODUCTION

Electrical extracellular stimulation (EES) of a central nervous system has been used empirically for several decades by electrophysiologists to explore fundamental properties of neural networks. Currently, peripheral nerve, deep brain, and spinal cord stimulation paradigms

Received 28 August 2013, Accepted 21 October 2013, Scheduled 22 October 2013

* Corresponding author: Zhi-Gong Wang (zgwang@seu.edu.cn).

are also used routinely for clinical restoration of lost motor function [1] and treatments of neurological disorders such as neuropathic pain [2], movement disorders, Parkinson disease [3], or epilepsy [4]. These healing strategies mainly use macroscopic implanted electrodes of several square millimeter to stimulate large regions of the central nervous system. More recently, microstimulation, which makes use of electrodes on the micron scale, is gaining increasing interest in both fundamental and clinical research, opening the possibility to stimulate small groups of neurons instead of large regions. For more than 35 years, MEAs provide a useful tool for neuroscientists to study the activity of large neuronal networks at a precision of single-cell activity, filling the gap between large-scale neural bioelectrical monitoring, such as electro- or magneto-encephalography measurements, and single-cell measurements, such as patch clamp techniques [5–7]. Microelectronic neural bridge, which includes microelectronic system and MEA-cuff array, was presented to connect the injured spinal cord to restore the perception and motor function of the spinal cord injury patients [8]. From the point of the view, MEAs are the focus of intensive developments [9–12]. These *in vitro* or *in vivo* microsystems increasingly benefit fundamental neuroscience aiming at understanding activity-dependent plasticity of neural networks, as well as clinical developments of efficient neural implants or prostheses.

Many EES obtained with MEAs have been reported, showing a great diversity of results [13–15]. However, despite a large body of literature on the EES, there is still a lack of knowledge on how an EES is related to the much better known transmembrane action voltage, and how to design the microelectrodes to stimulate, at best, the bioelectric activities. On the other hands, as reported recently, the activating of single neuron may strongly impact the activity of a large neural networks and even behavior [21, 22]. For this reason, determining optimal electrode configurations for efficient stimulation of a single neuron is the focus of current developments based on modeling approaches [23–26], where compartimentalized neurons are stimulated by modeled extracellular potential fields. The potential fields are calculated by solving the homogeneous partial differential equations under appropriate boundary conditions. Solutions to this problem can be derived analytically when the volume geometry and electrode configuration are simple [27–31]. However, when realistic geometries are considered, numerical simulations are required, such as finite element (FE) or finite difference models [24, 32–35].

The FE modeling studies have been dedicated to the understanding of electrical microstimulation of a single neuron using MEAs [36, 37] or neural tissues [38–40], opening the way to the design of MEA-based

neural prosthesis. Although they allow the simulation of complex 3-D microelectrode structure, these models cannot compute the bioelectrical activity of the neuron and the distribution of the electromagnetic field in the tissue in and out of the neuron at the same time. Normally, the geometry of the volume conductor such as the tissue in or around the neuron is implemented in an FE software, for example ANSYS or COMSOL. Then, a sophisticated model of the membrane biophysics, including voltage-dependent ionic currents, is implemented in the other transient response software, for instance NEURON or MATLAB. Recently, a new 3-D Finite-element model for MEA recording of extracellular action potential was presented. The approach is based on the thin-film approximation, which allows simulating the extracellular potential by means of a single transient computation, performed within a single FE software [41]. However, realistic extracellular stimulation means was not used in it.

The aim of the present study is twofold: First, a finite element model is validated for the realistic computation of the EES, and, second, it is studied how the configuration and position of the MEA affect the threshold for EES. This paper is thus divided into three parts. In the first part, a finite element model is developed for the calculation of the stimulated potential field incorporating the transmembrane voltage of the neuron membrane through nonlinear ordinary differential equations (ODEs) described by Hodgkin and Huxley(HH) [42]. In the second part of the paper, this model is used to evaluate the threshold of the EES for a straight fiber induced by four types of MEAs, i.e., mono-, bi-, tri-, and penta-polar arrays. Finally, the influences of the space between the microelectrodes in the array and the position of the MEA on the action potential stimulation are evaluated.

2. METHODS

The model of the EES presented here is a tool for studying the relationship between the transmembrane action voltage and extracellular stimulating potential, applied by means of an MEA in the extracellular medium. The computational model consists three main components: the electrical volume conductor (composed of the intracellular and extracellular media), the active neuron membrane, and the stimulating MEA.

2.1. Parametrical Geometry

A parametrical representation of the geometry of the neuron electrode interface in Figure 1 will be used. The neuron is represented by a 20-µm diameter spherical soma, a 10-µm-long hillock, with diameter

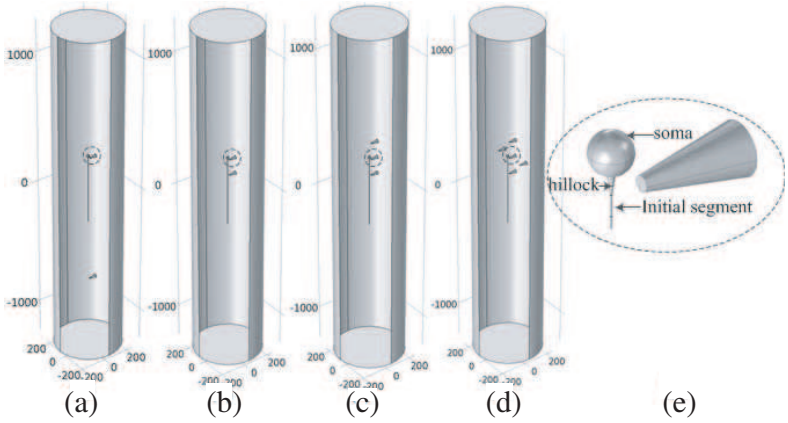

Figure 1. Three-dimensional FE domain, neuron structure, and MEAs. The neuron and microelectrode are in the center part of the cylinder. (a) Mono-polar MEA, (b) bi-polar MEA, (c) tri-polar MEA, (d) penta-polar MEA, (e) close-up of the soma, hillock, initial segment, axon, and the stimulating electrode nearby. Unit: μm.

tapering from 4 to 1 micron, and a 500-μm-long axon, both with 1-μm diameter.

These dimensions are chosen in accordance with the neuron described by Mainen et al. [43]. The cone style is roughly approximate to a normally used nonplanar electrodes [14–20]. Its tip angles are approximately 20 degree. The diameter of the base of the electrode and the height of each electrode is approximately 25 and 50 μm, respectively. The microelectrodes are positioned with a distance D_{c2e} on one side of the neuron. Mono-, bi-, tri-, and penta-polar MEAs are used. Each of them is composed of two kinds of microelectrodes: One is for stimulating and the others are grounded. The nervous tissue is represented by a 500-μm diameter and 2500-μm height cylindrical volume in Figure 1. The unique active neuron is in the center of the cylinder internal volume. The foregoing geometrical and electrical parameters are used throughout this paper. With the variation of the configuration and position of the microelectrode and the spacing between the microelectrodes of an array, the stimulating thresholds will be diverse and the effect of the stimulation will be compared.

2.2. Electrical Volume Conductor

The equations governing the behavior of the current and potential in the volume conductors are the Maxwell's equations. These equations

can be simplified because considering the size of the neuron structures and the time scale of the action potential, the instantaneous diffusion of magnetic field can be assumed [44]. Finally, Maxwell's equations can be replaced by the sole current conservation equation

$$\nabla \cdot \frac{\partial (\varepsilon \nabla \varphi)}{\partial t} + \nabla \cdot (\sigma \nabla \varphi) = 0 \tag{1a}$$

where φ, ε, and σ are the electrical potential, medium permittivity, and the medium conductivity, respectively. The intracellular and extracellular media are considered as purely resistive, homogeneous, and isotropic [32, 45]. The equation can also be written as

$$\varepsilon \left(\frac{\partial^3 \varphi}{\partial x^2 \partial t} + \frac{\partial^3 \varphi}{\partial y^2 \partial t} + \frac{\partial^3 \varphi}{\partial z^2 \partial t} \right) + \sigma \left(\frac{\partial^2 \varphi}{\partial x^2} + \frac{\partial^2 \varphi}{\partial y^2} + \frac{\partial^2 \varphi}{\partial z^2} \right) = 0 \tag{1b}$$

The value assigned to the extracellular conductivity is $0.3\,\mathrm{S/m}$ [45, 46] and the value assigned to the intracellular conductivity is $3\,\mathrm{S/m}$ [42]. The extracellular and intracellular permittivity are both $7.1 \times 10^{-10}\,\mathrm{AS/Vm}$.

The boundary condition of the model is that the potential on the outer boundary of the FE domain equals to zero since the fiber and the MEA in the center of the computational domain is very far from the outer boundary.

2.3. Thin-film Approximation of the Neuron Membrane

A neuron is an excitable cell that can be described as a semipermeable membrane with active, nonlinear, and inhomogeneous electrical properties, which separates the intracellular medium from the extracellular one. The neuronal membrane, being only a few nanometers thick, is very thin compared to the other typical dimensions which are in the micrometer range and above (e.g., neuron, microelectrode, etc.). This is troublesome for an FE implementation as meshing the membrane volume would result in unrealistic requirements in terms of computer processing power and memory resources. The thin-film approximation method is useful to get over this problem by avoiding the meshing of the membrane thickness [41]. It splitted the whole computational domain into two distinct meshed domains coupled through Neumann boundary conditions. The neuron membrane was thus replaced by the interface between the intracellular and extracellular spaces, where the Neumann boundary conditions, i.e., Equation (2a) and Equation (2b), are applied at the intracellular and the extracellular sides of the interface, respectively.

$$\sigma_{\mathrm{intra}} \nabla \varphi \cdot \mathbf{n} = i_{\mathrm{m}} (v_{\mathrm{m}}, t) \tag{2a}$$

$$\sigma_{\mathrm{extra}} \nabla \varphi \cdot \mathbf{n} = -i_{\mathrm{m}} (v_{\mathrm{m}}, t) \tag{2b}$$

where i_{m} and v_{m} are the transmembrane action current density and voltage, respectively. The present convention, where the transmembrane voltage is equal to the intracellular potential minus the extracellular potential, is adopted. Equation (2) make use of a model describing the transient relationship that couples the transmembrane potential and current density. The thin-film approximation is valid in any geometry under the assumptions that the membrane is negligibly thin and that the current flows perpendicularly through it. The transmembrane current density i_{m} can be determined by the classical semi-empirical set of nonlinear ODEs described by Hodgkin and Huxley (HH) [42]. It is expressed as the sum of the capacitive current (i_{C}), the ionic sodium (i_{Na}), the potassium current (i_{K}), and the leakage current densities (i_{L}), i.e.,

$$i_{\mathrm{m}} = i_{\mathrm{C}} + i_{\mathrm{Na}} + i_{\mathrm{K}} + i_{\mathrm{L}} \tag{3}$$

The expressions of i_{C}, i_{Na}, i_{K}, and i_{L} are

$$\begin{aligned} i_{\mathrm{C}} &= C_{\mathrm{m}} \frac{\mathrm{d}v_{\mathrm{m}}}{\mathrm{d}t},\ i_{\mathrm{Na}} = \bar{g}_{\mathrm{Na}} m^3 h \left(v_{\mathrm{m}} - E_{\mathrm{Na}}\right), \\ i_{\mathrm{K}} &= \bar{g}_{\mathrm{K}} n^4 \left(v_{\mathrm{m}} - E_{\mathrm{K}}\right),\ i_{\mathrm{L}} = \bar{g}_{\mathrm{L}} \left(v_{\mathrm{m}} - E_{\mathrm{L}}\right) \end{aligned} \tag{4}$$

where C_{m} is the membrane-specific capacitance, $\bar{g}_{\mathrm{Na}}$, $\bar{g}_{\mathrm{K}}$, and $\bar{g}_{\mathrm{L}}$ are the maximum ionic conductance density of sodium, potassium, and leakage ionic channels, respectively. Dimensionless ionic channel gating variables m, n, and h are computed using following ODE.

$$\frac{\mathrm{d}m}{\mathrm{d}t} = \alpha_{\mathrm{m}} (1-m) - \beta_{\mathrm{m}} m,\ \frac{\mathrm{d}n}{\mathrm{d}t} = \alpha_{\mathrm{n}} (1-n) - \beta_{\mathrm{n}} n,\ \frac{\mathrm{d}h}{\mathrm{d}t} = \alpha_{\mathrm{h}} (1-h) - \beta_{\mathrm{h}} h \tag{5}$$

The transfer rate coefficients α_{m}, β_{m}, α_{n}, β_{n}, α_{h}, and β_{h} are not constant. They are dependent on the transmembrane voltage. All the relative expressions are described as

$$\begin{aligned} \alpha_{\mathrm{m}} &= 1000 \frac{0.1 - 0.01v}{e^{(1-0.1v)} - 1},\ \beta_{\mathrm{m}} = 1000 \frac{0.125}{e^{0.0125v}},\ \alpha_{\mathrm{n}} = 1000 \frac{2.5 - 0.1v}{e^{(2.5-0.1v)} - 1} \\ \beta_{\mathrm{n}} &= 1000 \frac{4}{e^{v/18}},\ \alpha_{\mathrm{h}} = 1000 \frac{0.07}{e^{0.05v}},\ \beta_{\mathrm{h}} = 1000 \frac{1}{e^{(3-0.1v)} + 1} \end{aligned} \tag{6}$$

where $v = v_{\mathrm{m}} - v_{\mathrm{rest}}$, and v_{rest} is the resting potential and equals to $-60\,\mathrm{mV}$.

The values of the HH equation parameters are taken from [42] and shown in Table 1.

The maximum potassium and sodium conductance densities of the hillock and initial segment were exactly set to ten times the standard value in order to account for the larger concentrations of voltage-gated ionic channels in these structures and their greater excitability [41].

Table 1. Hodgkin and Huxley equations parameters.

ion	Reversal potential (mV)	Maximum ionic conductance density (mS/cm^2)	Membrane specific capacitance ($\mu F/cm^2$)
Na	45	120	1
K	−82	36	
L	−59.387	0.3	

These values are set arbitrarily in order to ensure the spike initiation in the hillock-initial segment area. A ratio of ten between the potassium and sodium conductance densities in the soma and in the hillock-initial segment is in the range used by Claverol-Tinture and Pine [47].

In summary, the whole model, strictly speaking, consists of two separated FE domains. The first one includes intracellular medium and the neuron membrane. The governing equation is (1) and the boundary condition is (2a). On the other hand, the extracellular medium, the MEA, the neuron membrane, and the outer boundary compose the second FE domain. The governing equation is (1) and the boundary conditions are (2b) and $\varphi = 0$, respectively. Both domains are coupled by Equation (2).

2.4. Finite-element Simulation

Four types of MEAs, i.e., mono-, bi-, tri-, and penta-polar MEAs, are used to study the relationship between the configuration of the MEA and the stimulating threshold. Furthermore, the position of the arrays is changed to confirm the validity of the conclusion. Three sets of parameters in Table 2 are used in the simulation. On the other hand, the space between the stimulating electrode and the grounded one D_{e2e} is also a major design parameter of array own. Its effect on the threshold is also studied. Besides the configuration and the spacing, the position of the MEA, which is defined by two parameters D_{O2o} and D_{c2e}, will also affect the stimulating threshold. The former is the distance between the center of the axon (marked by O) and the center between the stimulating electrode and its nether grounded one (marked by o). Given that the axis of the axon parallels the line determined by two centers of electrode tip surfaces, the distance between the axon and the microelectrode is defined as the spacing between the axis and such line. In Figure 2 and Table 2–4, the parameters of all modeled geometries are firstly illustrated and then summarized.

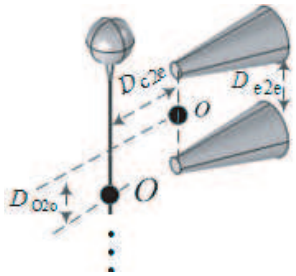

Figure 2. Parameters defined to describe the position of the MEA and the spacing between the electrodes.

Table 2. List of positions used for comparing the thresholds of fourtypes of MEAs (μm).

position	D_{e2e}	D_{O2o}	D_{c2e}
1		190	15
2	95	190	30
3		0	15

Table 3. List of spacing used for studying its influence of the spacing on the threshold (μm).

D_{e2e}	15	25	35	45	55	65	75	85	95	105	115	135	155	175
D_{O2o}	230	225	220	215	210	205	200	195	190	185	180	170	160	150
D_{c2e}	1 OR 5													

Simulation of extracellular stimulation was performed by application of a 52-ms voltage square pulse including a 1-ms rising edge and a 1-ms falling one through the extracellular electrode node.

The finite-element method (FEM) is well adapted to the solution of elliptic partial differential equations, such as the current conservation described by Equation (1), in complex 3-D geometries and when nonlinear phenomena occur. The computational domain is meshed with tetrahedral quadratic Lagrange finite elements. The reference mesh used in this study was comprised of approximately 10,000 elements and 25,000 degrees of freedom. The mesh was locally

Table 4. List of positions used for studying its influence on the threshold with the peta-polar MEA (μm).

D_{e2e}	D_{O2o}	D_{c2e}
95	The values from 30 to 280 with a spacing of 10	10
95	190	1, 2, and the values from 5 to 50 with a spacing of 5

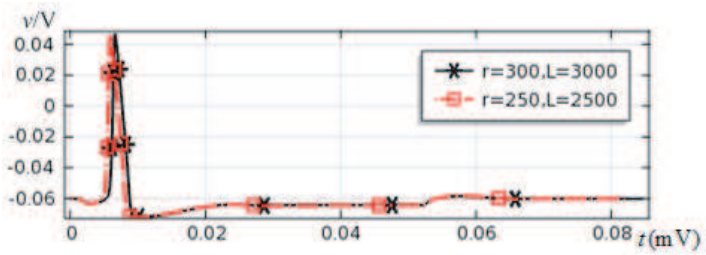

Figure 3. Two transmembrane voltages, simulated by placing the neuron in the volume conductor with (a) 250-μm radius and 2500-μm height and the one with (b) 300-μm radius and 3000-μm height.

refined to improve the simulation accuracy in the vicinity of the finest features of the geometry. The transient nonlinear FE simulations were performed with COMSOL Multiphysics 4.2 (COMSOL AB, Stockholm, Sweden). Each model was solved in a single computation using the DASPK algorithm [48], which uses an implicit time-stepping scheme with variable step size in COMSOL. The transient nonlinear computation of the reference model, performed on a Lenovo ThickPad L430 (Pentium(R) Core (TM) i5-2520M CPU 2.50 GHz 2.50 GHz), took about 250 s. The impacts of the FE domain size were verified. Two action potential, simulated by placing the neuron in the 250-μm radius, 2500-μm height volume conductor or in a larger 300-μm radius, 3000-μm height volume conductor, are almost indistinguishable (2.2% difference between the peak values and 5% delay), which has been illustrated in Figure 3.

3. RESULT

Firstly, the results in this section validate the feasibility of the presented neuron model. Then, the results show the influence of the configuration of the MEA on the excitation thresholds. Finally, the influences of three geometric parameters of the MEA, space between the microelectrodes, position of the array along the axon, and the distance between the axon and the array, on the stimulating thresholds are illustrated.

3.1. Validation of the Neuron Model

In order to validating the presented model including thin-film approximation of the neuron membrane, a simple example, which initial intracellular potential is set to 15 mV above the intracellular resting potential to trigger a transmembrane action voltage, is calculated in advance. The transmembrane action voltage and current obtained while solving foregoing three-dimensional FE model are compared with those obtained with the similar neuron model implemented in [41]. The two simulations provide almost identical results in terms of waveform and amplitude for the transmembrane action voltage and current (Figure 4).

3.2. Influence of the Configuration of MEA

Each of transmembrane voltage induced by five extracellular stimulating potentials is calculated to evaluate the threshold potential which can cause action potential for the mono-polar configuration.

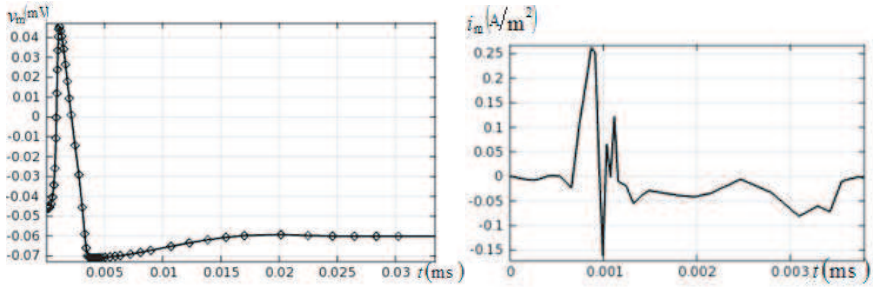

(a) (b)

Figure 4. (a) Represents the transmembrane potential v_m at the center of the axon for the FE model, (b) represents the transmembrane current density i_m at the center of the axon simulated by the FE model.

The thresholds of the other MEAs are also processed in this manner. Since the D_{c2e} and D_{O2o} may affect the threshold, the models with such different parameters are implemented in COMSOL. The foregoing method is repeated for each subsequent numerical trial. The parameters are shown in Table 2. The results are plotted in Fig. 5–7, which show the waveform of the transmembrane voltage stimulated with different extracellular potential through different MEA. The transmembrane voltage v_m stimulated the threshold potential is shown by red solid line with star. Three sets of the results illustrated that the penta-polar MEA has the lowest threshold, the tri-polar lower, the bi-polar higher, and the mono-polar highest.

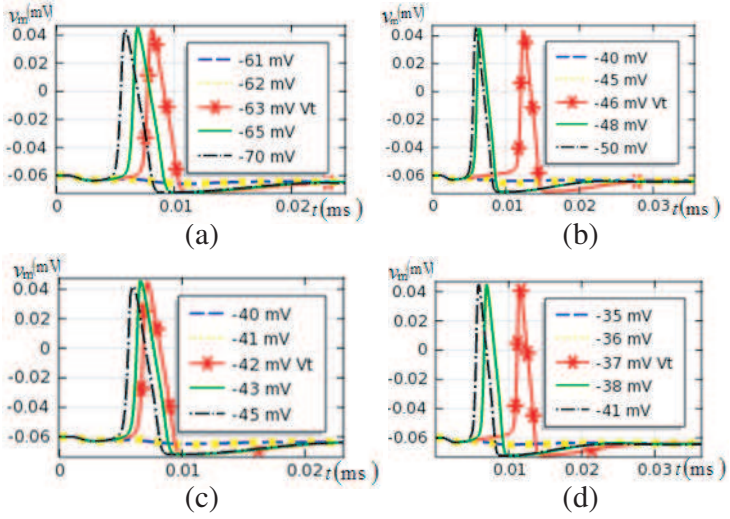

Figure 5. Simulation results of the stimulating threshold V_t from extracellular action potential stimulating model with 95-µm D_{e2e}, 190-µm D_{O2o} and 15-µm D_{c2e} (a) mono-polar MEA, (b) bi-polar MEA, (c) tri-polar MEA, and (d) penta-polar MEA.

3.3. Influence of the Spacing D_{e2e}

The ranges of D_{e2e} in Figure 8 are 15 µm to 175 µm, with a spacing of 10 or 20 µm. The distance D_{c2e} = 1 µm and 5 µm are used. The parameters used in the numerical trial are shown in Table 3. In Figure 8, the results show that the thresholds under different spacing almost equal to a constant. To be exact, fibre thresholds V_t have just a little higher values when D_{e2e} is larger.

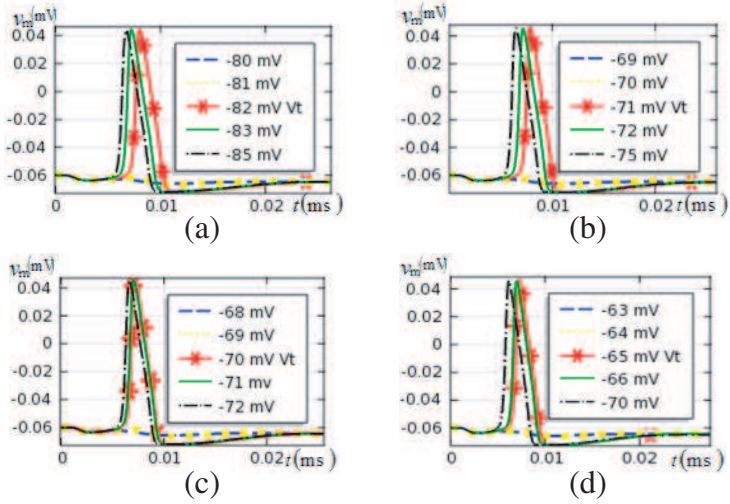

Figure 6. Simulation results of the stimulating threshold V_t from extracellular action potential stimulating model with 95-μm D_{e2e}, 190-μm D_{O2o} and 30-μm D_{c2e} (a) mono-polar MEA, (b) bi-polar MEA, (c) tri-polar MEA, and (d) penta-polar MEA.

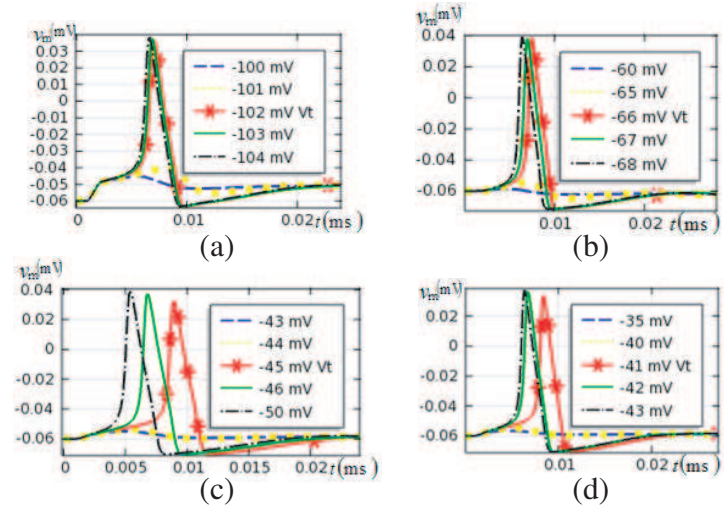

Figure 7. Simulation results of the stimulating threshold V_t from extracellular action potential stimulating model with 95-μm D_{e2e}, 0-μm D_{O2o} and 15-μm D_{c2e} (a) mono-polar MEA, (b) bi-polar MEA, (c) tri-polar MEA, and (d) penta-polar MEA.

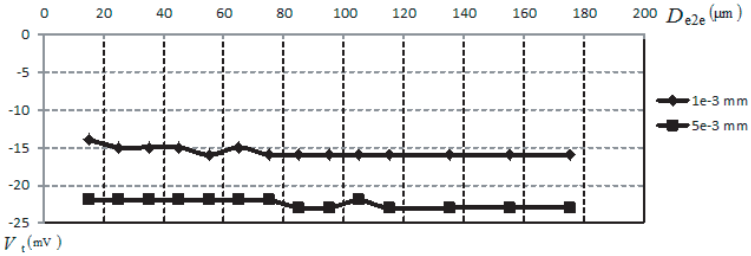

Figure 8. Relationship between the spacing of the electrodes in the penta-polar MEA and the extracellular stimulating threshold.

3.4. Influence of Distance D_{O2o}

The D_{O2o} is varied from 30 to 280 μm and the other parameters with $D_{c2e} = 15$ μm and $D_{e2e} = 95$ μm are used, which is shown in Table 4. The relationship between the position of the stimulating electrode and the relative parameter D_{O2o} is shown by arrows. The curve for threshold V_t versus D_{O2o} has been illustrated in Figure 9. The lowest threshold appears when the stimulating electrode exactly points to the center of the soma. Furthermore, all the thresholds in the range of a domain including soma, hillock, and initial segment are lower than the others.

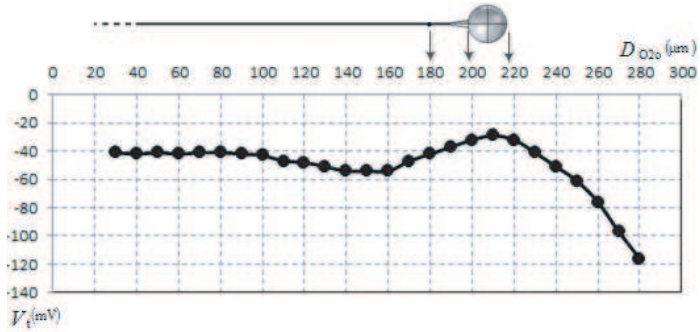

Figure 9. Relationship between the distance D_{O2o} and the extracellular stimulating threshold.

3.5. Influence of the Distance D_{c2e}

D_{c2e} is varied from 1 to 50 μm and the parameters with $D_{e2e} = 95$ μm and $D_{O2o} = 190$ μm are used, which is listed in Table 4. The relation between the V_t and D_{c2e} is shown in Figure 10. During the distance

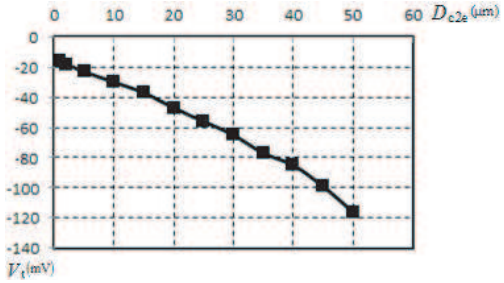

Figure 10. Relationship between the distance D_{c2e} and the extracesomallular stimulating threshold.

D_{c2e} increases, the threshold decreases nearly linearly at first and then exponentially.

4. DISCUSSION

This simulation study shows how microelectrode configuration and position influence the excitation threshold.

The first goal of this work is to estimate the effectiveness of stimulation for different electrode configurations. The stimulating threshold of the mono-polar configurations with a grounded electrode far away from the stimulating one is much higher than the one of the bi-polar one. Symmetrical configurations including tri-polar and penta-polar, which creates a more focal field than with asymmetrical mono-polar or bi-polar configuration stimulation, also requires lower stimulation thresholds than the mono-polar or bi-polar configuration (Figure 5–7). The threshold of penta-polar array is lowest. This is advantage of this MEA when considering chronic micro-stimulations, because conventional microelectrodes allow injecting only small currents to avoid electrode or tissue damage [49–51].

During the modeling for the different space between the electrodes, larger space displayed a little higher threshold. Therefore, decreasing the space between the stimulating electrode and the grounded one in a certain range can also decrease the stimulating threshold and lead to a more efficient stimulation.

The optimal stimulating position is not the point facing to the hillock and initial segments. Since the potassium and sodium conductance densities is ten times larger than the standard value, the stimulation with the MEA, which tip of the stimulating electrode points to the hillock and initial segment, maybe efficient. In reality, this guess is wrong. In the modeling study, the smallest threshold appears

in the condition that the stimulating microelectrode was pointed to the center of the soma. This phenomenon can be explained as follows: whether the action potential can be active or not depend on the activating function, which is the second derivative of the extracellular potential along the neuron. If the function is larger than zero, the action potential will be active, and if not, it will not. Therefore, when the stimulating electrode is exactly facing the hillock and initial segment, the activating function in the domain almost equals to zero and the large ion conductance densities cannot work.

The results for the relation between the threshold and the distance from the axon to the MEA show that the smaller the distance is, the lower the threshold is. Furthermore, the results illustrate how large the domain where the excited neurons exist is when a given stimulating potential is applied, which is valuable to the selective stimulation.

ACKNOWLEDGMENT

This work was supported by the National Natural Science Foundation of China (Grant Nos. 61001046 and 61076118).

REFERENCES

1. Gaunt, R. A. and A. Prochazka, "Control of urinary bladder function with devices: Successes and failures," *Progress in Brain Research*, Vol. 152, 163–194, 2006.
2. Winfree, C. J., "Spinal cord stimulation for the relief of chronic pain," *Curr. Surg.*, Vol. 62, No. 5, 476–481, Sep.–Oct. 2005.
3. Benabid, A. L., P. Pollak, C. Gervason, D. Hoffmann, D. M. Gao, et al., "Long term suppression of tremor by chronic stimulation of the ventral intermediate thalamic nucleus," *The Lancet*, Vol. 337, 403–406, Feb. 1991.
4. Theodore, W. H., "Brain stimulation for epilepsy," *Nat. Clin. Pract. Neurol.*, Vol. 1, No. 2, 64–65, Dec. 2005.
5. Thomas Jr., C. A., P. A. Springer, G. E. Loeb, Y. Berwald-Netter, and L. M. Okun, "A miniature microelectrode array to monitor the bioelectric activity of cultured cells," *Experiment. Cell Res.*, Vol. 74, No. 1, 61–66, 1972.
6. Wise, K. D., J. B. Angell, and A. Starr, "An integrated-circuit approach to extracellular microelectrodes," *IEEE Trans. Biomed. Eng.*, Vol. 17, No. 3, 238–247, Mar. 1970.
7. Buzsaki, G., "Large-scale recording of neuronal ensembles," *Nature Neurosci.*, Vol. 7, No. 5, 446–451, May 2004.

8. Wang, Z. G., X. S. Gu, X. Y. Lu, Z. L. Jiang, W. Y. Li, G. M. Lu, Y. F. Wang, X. Y. Shen, X. T. Zhao, H. L. Wang, Z. Y. Zhang, H. M. Shen, Y. Wua, W. X. Shen, J. Y. Zhang, D. Chen, X. Y. Mao, and H. X. Shen, "Microelectronics-embedded channel bridging and signal regeneration of injured spinal cords," *Progress in Natural Science*, Vol. 19, No. 10, 1261–1269, Oct. 2009.
9. Gross, G. W., A. N. Williams, and J. H. Lucas, "Recording of spontaneous activity with photoetched microelectrode surfaces from mouse spinal neurons in culture," *J. Neurosci. Methods*, Vol. 5, No. 1–2, 13–22, Jan. 1982.
10. Novak, J. L. and B. C. Wheeler, "Multisite hippocampal slice recording and stimulation using a 32 element microelectrode array," *J. Neurosci. Methods*, Vol. 23, No. 2, 149–159, Mar. 1988.
11. Charvet, G., L. Rousseau, O. Billoint, S. Gharbi, J. Rostaing, et al., "A 256-channel microelectrode array (MEA) system with integrated electronics for recording and stimulation of neural networks," *Society for Neuroscience 37th Annual Meeting, San Diego, California*, 171–174, USA, 2007.
12. Billoint, O., J. P. Rostaing, G. Charvet, and B. Yvert, "A 64-channel ASIC for in-vitro simultaneous recording and stimulation of neurons using microelectrode arrays," *Conf. Proc. IEEE Eng. Med. Biol. Soc.*, Vol. 1, 6070–6073, 2007.
13. Branner, A., R. B. Stein, and R. A. Normann, "Selective stimulation of cat sciatic nerve using an array of varying-length microelectrodes," *J. Neurophysiol*, Vol. 85, 1585–1594, 2001.
14. McCreery, D., A. Lossinsky, V. Pikov, and X. D. Liu, "Microelectrode array for chronic deep-brain microstimulation and recording," *IEEE Trans. Biomed. Eng.*, Vol. 53, No. 4, 726–737, Apr. 2006.
15. Smit, J. P. A., W. L. C. Rutten, and H. B. K. Boom, "Endoneural selective stimulating using wire-microelectrode arrays," *IEEE Trans. Biomed. Eng.*, Vol. 7, No. 4, 399-412, Dec. 1999.
16. Campbell, P. K., K. E. Jones, R. J. Huber, K. W. Horch, and R. A. Normann, "A silicon-based, three-dimensional neural interface: Manufacturing processes for an intracortical electrode array," *IEEE Trans. Biomed. Eng.*, Vol. 38, No. 8., 758–768, Aug. 1991.
17. Song, Y. K., W. R. Patterson, C. W. Bull, J. Beals, N. Hwang, A. P. Deangelis, C. Lay, J. L. McKay, A. V. Nurmikko, M. R. Fellows, J. D. Simeral, J. P. Donoghue, and B. W. Connors, "Development of a chipscale integrated microelectrode/microelectronic device for brain implantable neuroengineering applications," *IEEE*

Tans. Neural. System and Rehabilitation Eng., Vol. 13, No. 2, 220–226, Jun. 2005.

18. Hoogerwerf, A. C. and K. D. Wise, "A three-dimensional microelectrode array for chronic neural recording," *IEEE Trans. Biomed. Eng.*, Vol. 41, No. 12, 1136–1146, Dec. 1994.
19. Aziz, J. N. Y., R. Genov, B. L. Bardakjian, M. Derchansky, and P. L. Carlen, "Brain-silicon interface for high-resolution in vitro neural recording," *IEEE Tans. Biomedical Circuits and Systems*, Vol. 1, No. 1, 56–62, Mar. 2007.
20. Wang, R. X., X. J. Huang, G. F. Liu, W. Wang, F. T. Dong, and Z. H. Li, "Fabrication and characterization of a parylene-based three-dimensional microelectrode array for use in retinal prosthesis," *Journal of Microelectromechanical Systems*, Vol. 19, No. 2, 367–374, Apr. 2010.
21. Huber, D., L. Petreanu, N. Ghitani, S. Ranade, T. Hromadka, et al., "Sparse optical microstimulation in barrel cortex drives learned behaviour in freely moving mice," *Nature*, Vol. 451, No. 7174, 61–64, Jan. 2008.
22. Houweling, A. R. and M. Brecht, "Behavioural report of single neuron stimulation in somatosensory cortex," *Nature*, Vol. 451, 65–68, Jan. 2008.
23. Grumet, A. E., J. L. Wyatt, Jr, and J. F. Rizzo, 3rd, "Multi-electrode stimulation and recording in the isolated retina," *J. Neurosci. Methods*, Vol. 101, No. 1, 31–42, Aug. 2000.
24. Rattay, F. and S. Resatz, "Dipole distance for minimum threshold current to stimulate unmyelinated axons with microelectrodes," *IEEE Trans. Biomed. Eng.*, Vol. 54, No. 1, 158–162, Jan. 2007.
25. Holsheimer, J. and W. A. Wesselink, "Optimum electrode geometry for spinal cord stimulation: The narrow bipole and tripole," *Med. Biol. Eng. Comput.*, Vol. 35, No. 5, 493–497, Sep. 1997.
26. Rattay, F. and S. Resatz, "Effective electrode configuration for selective stimulation with inner eye prostheses," *IEEE Trans. Biomed. Eng.*, Vol. 51, No. 9, 1659–1664, Sep. 2004.
27. Meier, J. H., W. L. Rutten, A. E. Zoutman, H. B. Boom, and P. Bergveld, "Simulation of multipolar fiber selective neural stimulation using intrafascicular electrodes," *IEEE Trans. Biomed. Eng.*, Vol. 39, No. 2, 122–134, Feb. 1992.
28. Schnabel, V. and J. J. Struijk, "Evaluation of the cable model for electrical stimulation of unmyelinated nerve fibers," *IEEE Trans. Biomed. Eng.*, Vol. 48, No. 9, 1027–1033, Sep. 2001.

29. Fromherz, P., "Sheet conductor model of brain slices for stimulation and recording with planar electronic contacts," *Eur. Biophys. J.*, Vol. 31, No. 3, 228–231, Apr. 2002.
30. Church, P., A. Leduc, R. A. Beique, and J. R. Derome, "A numerical solution of cylindrical coordinate Laplace's equation with mixed boundary conditions along the axis of symmetry: Application to intracerebral stimulating electrodes," *J. Appl. Phys.*, Vol. 56, No. 1, 1–5, 1984.
31. Altman, K. W. and R. Plonsey, "Development of a model for point source electrical fibre bundle stimulation," *Med. Biol. Eng. Comput*, Vol. 26, No. 5, 466–475, Sep. 1988.
32. Buitenweg, J. R., W. L. Rutten, and E. Marani, "Extracellular stimulation window explained by a geometry-based model of the neuron-electrode contact," *IEEE Trans. Biomed. Eng.*, Vol. 49, No. 12, 1591–1599, Dec. 2002.
33. McIntyre, C. C., W. M. Grill, D. L. Sherman, and N. V. Thakor, "Cellular effects of deep brain stimulation: Model-based analysis of activation and inhibition," *J. Neurophysiol.*, Vol. 91, No. 4, 1457–1469, Apr. 2004.
34. Struijk, J. J., J. Holsheimer, and H. B. Boom, "Excitation of dorsal root fibers in spinal cord stimulation: a theoretical study," *IEEE Trans. Biomed. Eng.*, Vol. 40, No. 7, 632–639, Jul. 1993.
35. Laudani, A., S. Coco, and F. R. Fulginei, "Finite element model of charge transport across ionic channels," *COMPEL: The International Journal for Computation and Mathematics in Electrical and Electronic Engineering*, Vol. 32, No. 6, 1845–1854, 2013.
36. Buitenweg, J. R., W. L. C. Rutten, and E. Marani, "Geometry-based finite-element modeling of the electrical contact between a cultured neuron and a microelectrode," *IEEE Trans. Biomed. Eng.,* Vol. 50, No. 4, 501–509, Apr. 2003.
37. Buitenweg, J. R., W. L. C. Rutten, and E. Marani, "Modeled channel distributions explain extracellular recordings from cultured neurons sealed to microelectrodes," *IEEE Trans. Biomed. Eng.*, Vol. 49, No. 11, 1580–1590, Nov. 2002.
38. Heuschkel, M. O., M. Fejtl, M. Raggenbass, D. Bertrand, and P. Renaud, "A three-dimensional multi-electrode array for multi-site stimulation and recording in acute brain slices," *J. Neurosci. Methods*, Vol. 114, 135–148, 2002.
39. Joucla, S. and B. Yvert, "Improved focalization of electrical microstimulation using microelectrode arrays: A modeling study," *PLOS ONE*, Vol. 4, No. 3, e4828, 2009.

40. Joucla, S., P. Branchereau, D. Cattaert, and B. Yvert, "Extracellular neural microstimulation may activate much larger regions than expected by simulations: A combined experimental and modeling study," *PLOS ONE*, Vol. 7, No. 8, 41324, 2012.
41. Moulin, C., A. Glière, D. Barbier, S. Joucla, B. Yvert, P. Mailley, and R. Guillemaud, "A new 3-D finite-element model based on thin-film approximation for microelectrode array recording of extracellular action potential," *IEEE Trans. Biomed. Eng.*, Vol. 55, No. 2, 683–692, Feb. 2008.
42. Hodgkin, A. L. and A. F. Huxley, "A quantitative description of membrane current and its application to conduction and excitation in nerve," *J. Physiol.*, Vol. 117, 500–544, 1952.
43. Mainen, Z. F., J. Joerges, J. R. Huguenard, and T. J. Sejnowski, "A model of spike initiation in neocortical pyramidal neurons," *Neuron*, Vol. 15, 1427–1439, 1995.
44. Lindsay, K. A., J. R. Rosenberg, and G. Tucker, "From Maxwell's equations to the cable equation and beyond," *Progr. Biophys. Molecul. Biol.*, Vol. 85, No. 1, 71–116, May 2004.
45. Moffitt, M. A. and C. C. McIntyre, "Model-based analysis of cortical recording with silicon microelectrodes," *Clin. Neurophysiol.*, Vol. 116, No. 9, 2240–2250, Sep. 2005.
46. Holt, G. R. and C. Koch, "Electrical interactions via the extracellular potential near cell bodies," *J. Comput. Neurosci.*, Vol. 6, No. 2, 169–184, Mar.–Apr. 1999.
47. Claverol-Tinture, E. and J. Pine, "Extracellular potentials in low-density dissociated neuronal cultures," *J. Neurosci. Methods*, Vol. 117, 13–21, 2002.
48. Brown, P. N., A. C. Hindmarsh, and L. R. Petzold, "Using Krylov methods in the solution of large-scale differential-algebraic systems," *SIAM J. Scientif. Comput.*, Vol. 15, No. 6, 1467–1488, 1994.
49. McHardy, J., D. Geller, and S. B. Brummer, "An approach to corrosion control during electrical stimulation," *Ann. Biomed. Eng.*, Vol. 5, No. 2, 144–149, Jun. 1977.
50. McCreery, D. B., W. F. Agnew, T. G. Yuen, and L. Bullara, "Charge density and charge per phase as cofactors in neural injury induced by electrical stimulation," *IEEE Trans. Biomed. Eng.*, Vol. 37, No. 10, 996–1001, Oct. 1990.
51. Pudenz, R. H., L. A. Bullara, S. Jacques, and F. T. Hambrecht, "Electrical stimulation of the brain. III. The neural damage model," *Surg. Neurol.*, Vol. 4, No. 4, 389–400, Oct. 1975.